厚生労働科学研究費補助金（創薬基盤推進研究事業）
分担研究報告書

個体レベルでの発がん物質評価系の検証

分担研究者　津田　洋幸　名古屋市立大学・特任教授

Cre/loxP システムを用いた活性型ヒト $Hras^{G12V}$ トランスジェニックラット（Hras250）の肺にCreリコンビナーゼ発現アデノウイルスを感染させることによって、変異 ras 遺伝子の発現を誘導し肺がんを発生させた。発生した肺がんは、腺がん、扁平上皮がんあるいはそれらの混合した腺扁平上皮がんであった。特に、化学発がんで発生させることが困難な扁平上皮成分を含むがんをラットに高率に発生させることに成功したことから、Hras250 ラットは肺の扁平上皮がんの有用なモデルとなり得ると考えられた。

A．研究目的

肺癌は発生母地の違いとして小細胞がんと非小細胞がんに分類され、肺癌の約 80%は発生母地の不明な非小細胞癌（扁平上皮がん、腺がん、大細胞がん、その他のがん）とされる。疫学的には、扁平上皮癌および小細胞がんの発生には喫煙との関連が極めて強く、腺がんは非喫煙者にも発生する。肺がんにおける遺伝子変異は、Kras の変異は喫煙者に多く、非喫煙者ではEGFR の変異の頻度が高い。

肺がんの動物モデルとして、ラットには 2,2-dihydroxydi-n-propylnitrosamine（DHPN）、N-nitrosobis(2-hydroxypropyl)amine (BHP)、4-(Methyl-nitrosamino)-1-(3-pyridyl)-1-butanone (NNK) 等の発がん物質を投与するモデルがあり、マウスには NNK、urethane、4-Nitroquinoline-1-oxide （4-NQO）、2-amino-3,8-dimethylimidazo[4,5-f]quinoxaline (MeIQx) 等を投与し肺がんを誘発する化学発がんモデルがある。これら化学発がんモデルでは、主に腺がんが発生し、ヒトに多い扁平上皮がんの発生は稀である。化学発がんモデルでは、通常、発がん物質の投与後25ー50 週程度の期間が必要である。

我々は Cre リコンビナーゼにより活性型ヒト $Hras^{G12V}$ または $Kras^{G12V}$ が発現誘導されるトランスジェニックラット（Hras250、Kras301 およびKras327）を確立している（図1）。ラットはマウスに比べて体が大きく解析に充分な試料の採取が可能な点で優れている。先に記したように、化学発がんでは扁平上皮がんを発生させることは困難であり、試験期間も長期間となる。これを克服するために、Ras トランスジェニックラットを用いて、短期間に肺がんを発生させることが可能な新たな肺がんモデルの確立を行った。

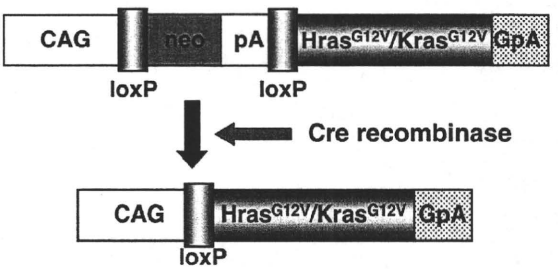

図 1　Hras250 および Kras301/327 ラットの導入遺伝子

B．研究方法

ラット肺がんの発生

Cre リコンビナーゼ発現アデノウイルスを HEK293 細胞に感染させて、Cre リコンビナーゼ発現アデノウイルスを増幅し精製した。精製した Cre リコンビナーゼ発現アデノウイルスを、Hras250 または Kras301/327 トランスジェニックラットの気管内に噴霧し（$4x10^9$ ifu/ml, 500 μl）、肺胞に感染させ

ることによって肺がんを発生させた。

病理解析

Hras250 またはKras301/327 ラットの肺にCre リコンビナーゼ発現アデノウイルスを感染させ、2-4 週後に肺組織を採取し、ホルマリンまたはパラホルムアルデヒドで固定した。パラフィン包埋後、薄切しH&E 染色を行った。

(倫理面への配慮)

本研究は、遺伝子組み換え実験においては「名古屋市立大学大学院医学研究科遺伝子組み換え実験等安全委員会」、動物実験においては「名古屋市立大学大学院医学研究科動物実験に関する指針」に基づく「動物委員会」の承認を経て実施された。

C．研究結果

気管内噴霧スプレーを用いて Cre リコンビナーゼ発現アデノウイルスを Hras250 またはKras301/327 ラットの肺内に投与した。Hras250 ラットでは 3ー6 週後に肺に多数の結節がみられた。一方、Kras301/327 ラットでは、4ー8 週経過後においても肉眼的な変化は観察されなかった。

病理組織学的検査により、Hras250 ラットでは、2 週後より小型の増殖性病変が肺全体に散発性にみられ、3 週後より大型の結節性病変がみられた。これら結節性の病変は腺がん、または扁平上皮がんであった。初期の増殖性病変は肺胞 II 型細胞のマーカーであるSP-C 陽性、またはクララ細胞のマーカーであるCC10 陽性であった。腺がん、扁平上皮がんにおいてはCC10 陽性細胞はみられたが、SP-C 陽性細胞は全くみられなかった。

Kras301/327 ラットでは肺胞の過形成から腺腫はみられたが、Hras250 ラットでみられた腺がん、扁平上皮がんは 8 週後においてもみられなかった。

D．考察

従来、末梢肺では II 型肺胞上皮細胞、クララ細胞、あるいはこれら両者に共通の前駆細胞が幹細胞の候補とされ、これら細胞が末梢肺がん発生母細胞と考えられてきた。本肺がんモデルでは、II 型肺胞上皮細胞のマーカーである SP-C は初期病変では陽性であるが、がん部において検出されなかったことから、II 型肺胞上皮細胞からはがんは発生しないと推測された。クララ細胞のマーカーである CC10 は初期病変からがんに至るまで発現がみられたことから、クララ細胞に由来すると考えられた。したがって、Hras250 ラット肺がんモデルにおいて、クララ細胞より肺腺がんおよび扁平上皮がんは発生すると考えられた。

活性型 Hras 単独で肺がんが発生したのに対し、活性型 Kras 単独では肺がんが発生しなかった理由は不明であるが、今後、活性型 Ras の発現量やシグナル伝達の相異を検討したい。

扁平上皮がんは、腺がんについで発生頻度が高く、男性の肺がんのうち約 40%、女性では約 15%、全体では 30%程度を扁平上皮がんが占めていることから、本モデルの有用性は高いと考えられる。

E．結論

我々の Hras250 ラット肺がんモデルにおいて、特に化学発がんでは発生させることが困難な扁平上皮成分を含むがんが短期間に発生させることが可能となった。さらに、腺がん・扁平上皮がんの起始細胞として、クララ細胞が考えられた。Hras250 ラットでは、特に化学発がんでは発生させることが困難な扁平上皮成分を含む肺がんが短期間に発生することから、本モデルはヒト肺がんモデルとして有用である。

F．健康危険情報

特記すべき事無し。

G．研究発表

（1）論文発表

該当無し

（2）学会発表

該当無し

H．知的所有権の出願・登録状況

該当なし

研究成果の刊行に関する一覧表

雑誌

発表者氏名	論文タイトル名	発表誌名	巻号	ページ	出版年
Okudaira N, Iijima K, Koyama T, Minemoto Y, Kano S, Mimori A, Ishizaka Y.	Induction of long interspersed nucleotide element-1 (L1) retrotransposition by 6-formylindolo[3,2-b]carbazole (FICZ), a tryptophan photoproduct.	*Proc Natl Acad Sci U S A.*	107	18487-18492	2010

Induction of long interspersed nucleotide element-1 (L1) retrotransposition by 6-formylindolo[3,2-*b*] carbazole (FICZ), a tryptophan photoproduct

Noriyuki Okudaira[a,b], Kenta Iijima[a], Takayoshi Koyama[a], Yuzuru Minemoto[a], Shigeyuki Kano[a,b], Akio Mimori[a], and Yukihito Ishizaka[a,1]

[a]National Center for Global Health and Medicine, Shinjuku-ku, Tokyo 162-8655, Japan; and [b]Graduate School of Comprehensive Human Sciences, University of Tsukuba, Tsukuba 305-8577, Japan

Edited* by George R. Stark, Lerner Research Institute, Cleveland, OH, and approved August 24, 2010 (received for review February 5, 2010)

Long interspersed nucleotide element-1 (L1) is a retroelement comprising about 17% of the human genome, of which 80–100 copies are competent as mobile elements (retrotransposition: L1-RTP). Although the genetic structures modified during L1-RTP have been clarified, little is known about the cellular signaling cascades involved. Herein we found that 6-formylindolo[3,2-*b*]carbazole (FICZ), a tryptophan photoproduct postulated as a candidate physiological ligand of the aryl hydrocarbon receptor (AhR), induces L1-RTP. Notably, RNA-interference experiments combined with back-transfection of siRNA-resistant cDNAs revealed that the induction of L1-RTP by FICZ is dependent on AhR nuclear translocator-1 (ARNT1), a binding partner of AhR, and the activation of cAMP-responsive element-binding protein. However, our extensive analyses suggested that AhR is not required for L1-RTP. FICZ stimulated the interaction of the L1-encoded open reading frame-1 (ORF1) and ARNT1, and recruited ORF1 to chromatin in a manner dependent on the activation of mitogen-activated protein kinase. Along with our additional observations that the cellular cascades for FICZ-induced L1-RTP were different from those of L1-RTP triggered by DNA damage, we propose that the presence of the cellular machinery of ARNT1 mediates L1-RTP. A possible role of ARNT1-mediated L1-RTP in the adaptation of living organisms to environmental changes is discussed.

ARNT1 | ORF1 | cAMP-responsive element-binding protein | MAPK | chromatin recruitment

About 45% of the human genome is composed of transposable elements (1, 2). Long interspersed nucleotide element-1 (LINE-1; L1) is the most abundant component of retroelements, comprising about 17% of the human genome (1, 3). Its structural alignment is conserved from fish to human with two encoded proteins, open reading frames 1 and 2 (ORF1 and 2), the molecular weights of which are about 40 and 150 kDa, respectively (3, 4). ORF1 is a basic protein that binds mRNA, whereas ORF2 has dual functions of endonuclease and reverse-transcriptase activities (3). ORF1 and 2 can complete the retrotransposition of L1 (L1-RTP), which is processed by three steps: transcription, reverse transcription, and the insertion of newly synthesized L1-DNA into the host genome by target-primed reverse transcription (3). Among about 5×10^5 copies of human L1, 80–100 copies are competent as mobile elements (5), and genome shuffling by L1-RTP generates unique expression profiles depending on the integration sites of newly synthesized L1 DNA (6). DNA damage is a reported trigger of L1-RTP (7), but the cellular cascades involved or other factors responsible for the induction of L1-RTP are largely unknown.

The aryl hydrocarbon receptor (AhR), a basic helix–loop–helix/Per–Arnt–Sim (bHLH/PAS) transcription factor, is conserved in invertebrates to human (8, 9), and it recognizes various polycyclic aromatic hydrocarbons (10). For example, 2,3,7,8-tetrachlorodibenzo-*p*-dioxin (TCDD), a well-characterized AhR ligand, induces heterodimer formation (AhR complex; AHRC) of AhR and AhR nuclear translocator-1 (ARNT1). Depending on the nuclear localization signal (NLS) of ARNT1 (11), AHRC is translocated to the nucleus, recognizes the xenobiotic response element (XRE), and induces gene expression such as *CYP1A1* mRNA (12). Sequence similarities among species and physiological functions support the idea that AHRC was an innovation in vertebrates that enabled them to metabolize xenobiotics in their environments (8). However, its real function remains elusive due to a lack of definite information about its authentic ligands (8, 12).

As a candidate physiological AhR ligand, 6-formylindolo[3,2-*b*]carbazole (FICZ) is of particular interest. FICZ is generated from tryptophan by ultraviolet B irradiation (13, 14), and its metabolite has been identified in human urine (15). FICZ has a high affinity for AhR (13) and induces *CYP1A1* mRNA depending on the AhR (14, 16). Intriguingly, studies have proposed recently that FICZ and TCDD are differentially involved in T-cell differentiation: FICZ generates proinflammatory T cells (T_H17), whereas TCDD induces regulatory T cells (T_{reg}) (17, 18). These observations suggest that AhR ligands have novel, uncharacterized biological functions.

In the current study, we found that FICZ induced L1-RTP and that the induction of L1-RTP by FICZ depended on ARNT1, but not on AhR. Biochemical analysis revealed that FICZ activated mitogen-activated protein kinase (MAPK) and phosphorylated cAMP-responsive element-binding protein (CREB) (19), both of which were required for L1-RTP. Furthermore, FICZ induced the association of ORF1 and ARNT1, and recruited ORF1 to chromatin. These data suggest the presence of ARNT1-mediated genome shuffling by L1-RTP, and we discuss its possible involvement in the adaptation of living organisms to environmental changes.

Results

FICZ Induces L1-RTP. We first assessed FICZ-induced L1-RTP by a colony assay using pCEP4/L1*mneo*I/ColE1 (pL1-Neo^R) (20); its schematic representation is depicted in Fig. 1*A*. pL1-Neo^R contains all the components of the L1 gene and an inversely inserted transcriptional unit encoding a neomycin-resistant (Neo^R) gene as a reporter. The Neo^R gene had sequences of splicing donor (SD) and splicing acceptor (SA) in a sense orientation (*SI Methods*). The effects of FICZ on HuH-7 and HeLa cells were examined according to the experimental protocol (Fig. 1*A Lower*). As shown

Author contributions: N.O., S.K., A.M., and Y.I. designed research; N.O., T.K., and Y.I. performed research; N.O., K.I., T.K., and Y.M. contributed new reagents/analytic tools; N.O., T.K., and Y.I. analyzed data; and Y.I. wrote the paper.

The authors declare no conflict of interest.

Freely available online through the PNAS open access option.

*This Direct Submission article had a prearranged editor.

See Commentary on page 18239.

[1]To whom correspondence should be addressed. E-mail: zakay@ri.ncgm.go.jp.

This article contains supporting information online at www.pnas.org/lookup/suppl/doi:10.1073/pnas.1001252107/-/DCSupplemental.

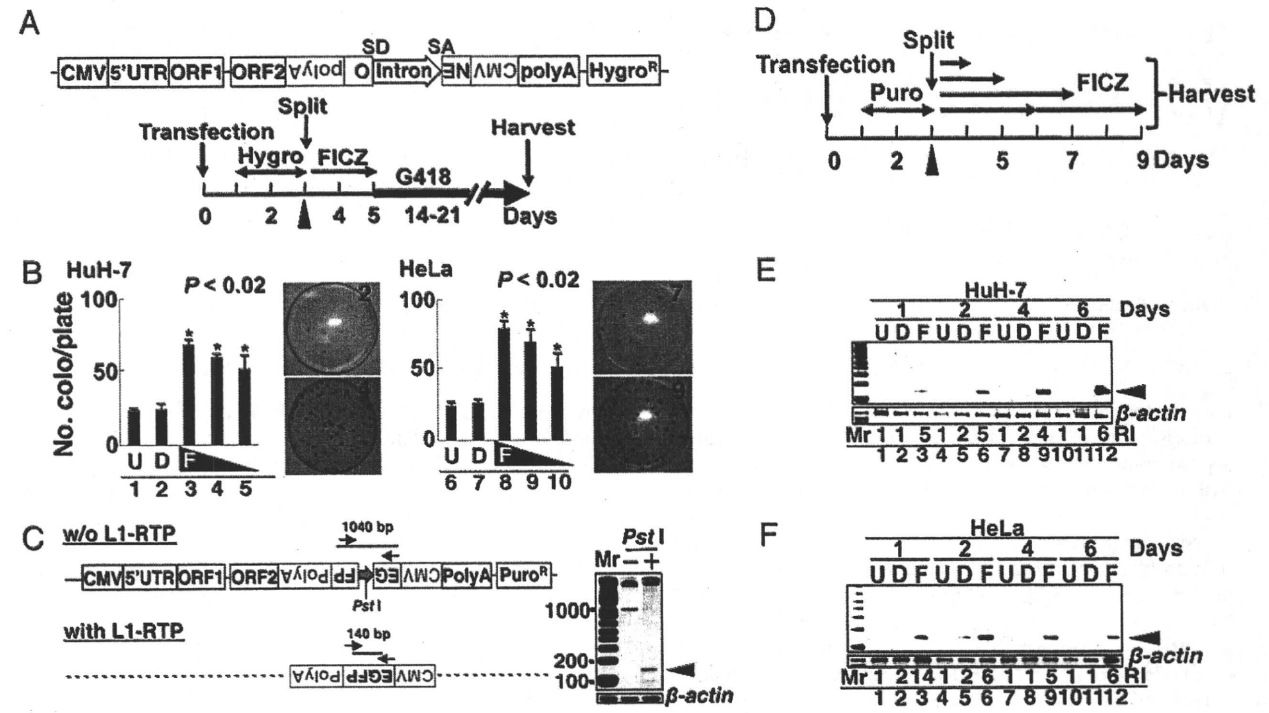

Fig. 1. FICZ induces L1-RTP. (*A*) Schematic diagram of pL1-Neo^R and the experimental protocol for the colony assay. Cells were transfected with pL1-Neo^R, selected for 2 d using Hygro, and exposed for 2 d to FICZ. Selection with G418 started on day 5. In some experiments, siRNAs of target genes were transfected on day 3 (arrowhead) followed by exposure to FICZ on the next day (*SI Methods*). (*B*) Colony assay results. Cells were treated with no reagents (U, lanes 1 and 6), 0.01% dimethyl sulfoxide (DMSO; D, lanes 2 and 7), or FICZ at 100, 10, and 1 nM (F, lanes 3–5 and 8–10). The numbers of colonies were normalized by viability (Fig. S1*A*). The mean numbers of colonies ± standard deviation (SD) are shown. Asterisks indicate statistical significance ($P < 0.02$). Stained plates are also shown. Plate numbers 2 and 4 are for HuH-7 cells and plate numbers 7 and 9 are for HeLa cells. The upper and lower plates revealed Neo^R colonies formed by 0.01% DMSO (2 and 7) or 10 nM FICZ (4 and 9), respectively. (*C*) Schematic diagram of pEF06R and the rationale for the PCR-based assay. pEF06R has a structure similar to that of pL1-Neo^R except for *EGFP* cDNA instead of the Neo^R gene. PCR primers targeting separate exons of *EGFP* cDNA (arrows) amplify a 1,040-bp or 140-bp fragment, depending on the induction of L1-RTP. The dotted line indicates the presence of similar structure of pEF06R. To selectively amplify the 140-bp band, DNA samples were treated with PstI (whose site is present in the intron) (*Right*, lane 2). (*D*) Experimental protocols for the PCR-based assays (*SI Methods*). After transfection of pEF06R, HuH-7 cells were cultured for 2 d in the presence of Puro. After exposure for 1–6 d to 10 nM FICZ, genomic DNAs were prepared and subjected to PCR-based analysis of L1-RTP. (*E* and *F*) Results of the PCR-based assays. Both HuH-7 (*E*) and HeLa (*F*) cells showed the amplified 140-bp band within 1 d after FICZ treatment (arrowheads). Relative intensities (RI) were calculated based on signal intensities of the 140-bp DNA and a DNA fragment of *β-actin* amplified as an internal control. D, 0.001% DMSO; F, 10 nM FICZ; U, untreated.

in Fig. 1*B*, L1-RTP was induced in both cell lines by FICZ at concentrations of 100, 10, and 1 nM (Fig. 1*B*, lanes 3–5 and 8–10; $P < 0.02$). No cytotoxic effects of the compound were detected even at 100 nM FICZ (Fig. S1*A*).

The induction of L1-RTP by FICZ was confirmed by a PCR-based assay with pEF06R (*SI Methods*) (7). As shown in Fig. 1*C*, PCR primers were designed in separate exons of *EGFP* cDNA, such that a 140-bp fragment would be amplified when L1-RTP was induced (Fig. 1*C*). By treating the sample DNAs with PstI (the site is present in the intron), the 140-bp band was selectively amplified (Fig. 1*C Right*, lane 2). According to the protocol shown in Fig. 1*D*, we carried out a time-course analysis of FICZ-induced L1-RTP. When 10 nM FICZ was applied, both HuH-7 cells and HeLa cells showed the 140-bp band within 1–2 d (Fig. 1 *E* and *F*). Additionally, the frequency of FICZ-induced L1-RTP was 10^{-4} to 10^{-5}, when estimated by the PCR-based assay (Fig. S1*B*).

FICZ-Induced L1-RTP Under Down-Regulation of Endogenous AhR. Because FICZ is an AhR ligand (14, 15), we examined whether AhR is required for FICZ-induced L1-RTP. As an initial experiment, we verified the effects of 3′-methoxy-4′-nitroflavone (MNF), an inhibitor of AhR (16). Notably, MNF did not reduce the FICZ-induced L1-RTP (Fig. S1*C*, lane 6), although it abolished the induction of *CYP1A1* mRNA (Fig. S1*D*, lane 6). Data strongly suggested that AhR is not required for the induction of L1-RTP by FICZ. To prove this, we carried out RNA-interference experiments using *AhR* siRNA. First, we confirmed that all three *AhR* siRNAs prepared, when used at 10 nM, could down-regulate the endogenous AhR to a level less than 20% that of the control (Fig. 2*A*; see also Fig. S2*A*). Then, we examined the effects of *AhR* siRNAs on the induction of L1-RTP by FICZ. Intriguingly, the induction of L1-RTP was observed even in the presence of these siRNAs (Fig. 2*B*; left and right panels depict the results with *AhR* siRNA-1 and -3, respectively). To gain further evidence, we carried out experiments under more stringent conditions. When 50 nM *AhR* siRNA was transfected into HuH-7 cells, the endogenous AhR was strongly suppressed for at least 3 d (Fig. 2*C*, lane 6). We next examined the effects of 2-d treatment of FICZ, and G418 selection was immediately started after FICZ exposure (Fig. 1*A*). Even under such conditions, FICZ induced L1-RTP (Fig. 2*D*, lane 6). Additionally, the activities of low doses of FICZ (1 and 0.1 nM) were examined under similar conditions (50 nM *AhR* siRNA) and again, the PCR-based assay detected L1-RTP (Fig. 2*E*, lanes 11 and 12). By transfecting 10 nM *AhR* siRNA, the induction of *CYP1A1* mRNA expression by FICZ was completely abolished (Fig. 2*F*, lane 9), indicating that endogenous AhR was functionally eliminated by the siRNA, although the residual amount of AhR was detectable.

Based on these data, we concluded that the induction of L1-RTP by FICZ is independent of AhR.

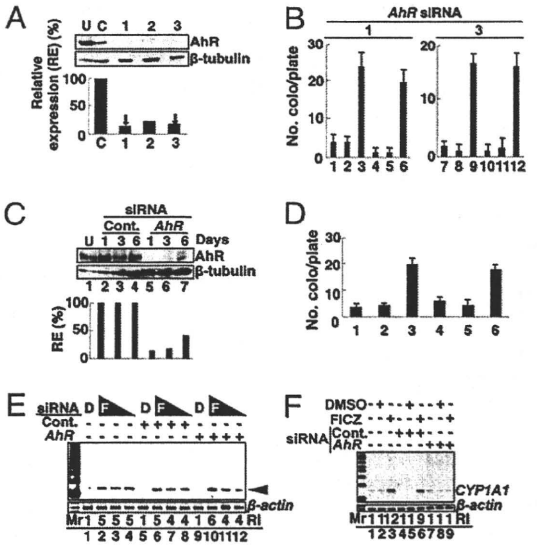

Fig. 2. AhR is dispensable for FICZ-induced L1-RTP. (*A*) Functional evaluation of *AhR* siRNAs. First, dose responses of *AhR* siRNAs for the suppression of endogenous AhR were verified (Fig. S2*A*). Then, the activities of three different *AhR* siRNAs (1–3) at 10 nM were examined. Relative expression (RE) of the AhR protein was calculated based on the expression levels of the proteins in the presence of control and *AhR* siRNAs. The RE was 11%, 19%, and 14% after transfection with *AhR* siRNA-1, -2, and -3, respectively. Arrows indicate the siRNAs used for the following experiments. (*B*) *AhR* siRNAs did not suppress FICZ-induced L1-RTP. Results of the colony assay performed in the presence of control siRNA (lanes 1–3 and 7–9) or *AhR* siRNAs (lanes 4–6 and 10–12 for siRNA-1 and -3, respectively) are shown. HuH-7 cells were treated with no reagents (lanes 1, 4, 7, and 10), 0.001% DMSO (lanes 2, 5, 8, and 11), or 10 nM FICZ (lanes 3, 6, 9, and 12). Mean numbers of colonies ± SD are shown. (*C*) Efficient suppression of endogenous AhR by siRNA. Western blot analysis was performed on days 1, 3, and 6 following the transfection of 50 nM *AhR* siRNA-1. The RE of AhR protein was calculated and plotted, indicating 13%, 16%, and 40% observed on day 1, 3, and 6 after transfection with *AhR* siRNA-1, respectively. Cont., control; U, untreated. (*D*) FICZ induced L1-RTP under stringent conditions. A colony assay was performed following the introduction of 50 nM control siRNA (lanes 1–3) or *AhR* siRNA-1 (lanes 4–6). HuH-7 cells were treated with no reagents (lanes 1 and 4), 0.001% DMSO (lanes 2 and 5), or 10 nM FICZ (lanes 3 and 6). G418 selection started immediately after FICZ treatment. Mean numbers of colonies ± SD are shown. (*E*) Low doses of FICZ induced L1-RTP under stringent conditions. On day 2 following the introduction of 50 nM control siRNA (lanes 5–8) or *AhR* siRNA-1 (lanes 9–12), HuH-7 cells were treated for 2 d with FICZ at 10 nM (lanes 2, 6, and 10), 1 nM (lanes 3, 7, and 11), or 0.1 nM (lanes 4, 8, and 12). Results of the PCR-based assay performed on the second day of FICZ treatment are shown. The arrowhead indicates L1-RTP. The RI of the 140-bp band was also calculated. (*F*) *AhR* siRNA suppressed *CYP1A1* mRNA expression. RT-PCR done on day 2 after introduction of 10 nM control siRNA (lanes 4–6) or *AhR* siRNA-1 (lanes 7–9) is shown. Cells were treated for 6 h with 10 nM FICZ and subjected to analysis. The RI was calculated based on the signal intensities of the transcript by the control and *AhR* siRNAs.

FICZ-Induced L1-RTP Is Dependent on ARNT1. Next, we examined the involvement of ARNT1 and observed that two different *ARNT1* siRNAs (1 and 2) efficiently suppressed the expression of endogenous ARNT1 (Fig. 3*A*; data with siRNA-1 and -2 are shown; see also Fig. S2*B*), and both siRNAs completely abolished FICZ-induced L1-RTP (Fig. 3*B*). The PCR-based assay also detected the inhibitory effects of the siRNA (Fig. S3*A*, lane 9), and the expression of *CYP1A1* mRNA was also inhibited by the siRNA (Fig. 3*C*, lane 9). Data suggested that the siRNA abrogated the function of endogenous ARNT1 and inhibited L1-RTP. To confirm this, we carried out a back-transfection experiment using siRNA-resistant *ARNT*1 cDNA (21). First, we confirmed that the introduction of a plasmid DNA expressing an siRNA-resistant *Flag-tagged ARNT1* mRNA (pSi^{R}-*ARNT1*; *SI Methods*) could restore the protein expression that had been reduced by the siRNA (Fig. 3*D*, lane 4). Then, we observed that pSi^{R}-*ARNT1* recovered the formation of Neo^{R} colonies, which had been suppressed by the siRNA (Fig. 3*E*, compare lanes 6 and 9; *SI Methods*). These data indicated that ARNT1 is involved in FICZ-induced L1-RTP.

To exclude the possibility that other cellular proteins related to the activity of AHRC are involved in FICZ-induced L1-RTP, we examined the effects of 10 nM siRNAs of *AhRR* (22) and *ARNT2* (23) on L1-RTP (Fig. S2 *C* and *D*). The results revealed that these molecules are not required for FICZ-induced L1-RTP (Fig. S3*B*, lanes 9 and 12).

Involvement of MAPK and CREB in the Induction of L1-RTP by FICZ. As TCDD activates MAPK (24), we tested the phosphorylation of MAPK substrates possibly related to the induction of L1-RTP. Among the three MAPK substrates examined, CREB was phosphorylated by FICZ (Fig. 4*A*, lane 3), whereas C/EBP-β and c-Jun were not (Fig. 4*A*). Notably, the FICZ-induced phosphorylation of CREB was abolished by the down-regulation of ARNT1 by siRNA (Fig. 4*B*, lane 6). We then examined the effects of MAPK inhibitors on FICZ-induced L1-RTP. As shown in Fig. 4*C*, the MAPK inhibitors, SB202190 for p38 (25) and SP600125 for JNK (26), efficiently suppressed L1-RTP (compare lanes 3, 6, and 7). The PCR-based assay revealed similar results, indicating the involvement of MAPK in FICZ-induced L1-RTP (Fig. S3*C*, lanes 6, 8, and 10).

To obtain direct evidence of the requirement of CREB for L1-RTP, the effects of *CREB* siRNAs were examined. Two different *CREB* siRNAs, which efficiently suppressed the expression of endogenous CREB protein (Fig. 3*D*, lanes 1 and 2), blocked L1-RTP (Fig. 4*E*; data with siRNA-1 and -2 are shown; see also Fig. S2*C*). Again, the PCR-based assay gave similar results (Fig. S3*D*, lane 9). Moreover, a plasmid DNA expressing an siRNA-resistant *Flag-tagged CREB* mRNA (pSi^{R}-*CREB*) successfully restored both CREB expression (Fig. 4*F*, lane 4) and L1-RTP (Fig. 4*G*, compare lanes 6 and 9). These data indicated that in response to FICZ, ARNT1 modulates the activity of MAPK, phosphorylates CREB, and induces L1-RTP.

Interestingly, SP600125 abrogated the induction of L1-RTP by FICZ, but we did not observe that FICZ induced the phosphorylation of c-Jun. Although SP600125 was originally proposed as a specific inhibitor of JNK (26), it was ascertained by subsequent studies that the compound could inhibit activities of several other protein kinases such as SGK, p70 ribosomal protein S6 kinase, AMPK, CDK2, and CK1δ (27). Data suggest the presence of an uncharacterized substrate(s), the activation of which is critical for L1-RTP by FICZ and sensitive to SP600125.

Chromatin Recruitment of ORF1 by FICZ-Dependent Activation of MAPK. Recently, Goodier et al. reported that ORF1, originally localized in cytoplasmic stress granules, is translocated to chromatin in response to stress stimuli (28). This led us to hypothesize that FICZ induces the nuclear trafficking of ORF1. To demonstrate this, we introduced a plasmid DNA encoding a chimeric protein composed of a codon-optimized ORF1 (29) tagged with a motif for tandem affinity purification (TAP) (30) into HuH-7 cells (*SI Methods*) and examined the FICZ-induced chromatin recruitment of ORF1. Western blot analysis revealed that FICZ increased ORF1 in the chromatin fraction (Fig. 5*B*, lane 2), although a slight amount of ORF1 was originally present in the chromatin fraction (Fig. 5*A*, lane 3). FICZ induced no increase in cellular ORF1 (Fig. S4 *A* and *B*) or ORF2 (Fig. S4 *C* and *D*). Immunoprecipitation followed by Western blot analysis revealed that FICZ triggered the complex formation of ORF1 and ARNT1 (Fig. 5*C*, compare lanes 4 and 8). Moreover, the MAPK inhibitor attenuated the FICZ-induced chromatin recruitment of ORF1 (Fig. 5*D*, compare lanes 3 and 6). Along with observations that the level of endogenous ARNT1 was not changed by FICZ (Fig. S4*E*),

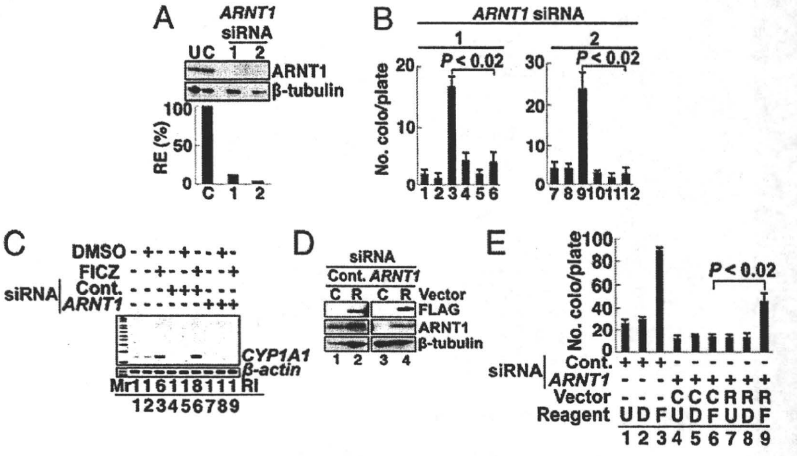

Fig. 3. ARNT1 is required for FICZ-induced L1-RTP. (*A*) Functional evaluation of *ARNT1* siRNAs. First, dose responses of *ARNT1* siRNAs for the suppression of endogenous ARNT1 were verified (Fig. S2*B*). Then, the activities of two different *ARNT1* siRNAs (1 and 2) at 10 nM were examined. The RE of endogenous ARNT1 protein was 12% and 4% when *ARNT1* siRNA-1 and -2 were introduced, respectively. (*B*) *ARNT1* siRNAs abrogated L1-RTP. A colony assay was performed on HuH-7 cells following the introduction of control siRNA (lanes 1–3 and 7–9) or *ARNT1* siRNA-1 and -2 (lanes 4–6 and 10–12). Cells were treated with no reagents (lanes 1, 4, 7, and 10), 0.001% DMSO (lanes 2, 5, 8, and 11), or 10 nM FICZ (lanes 3, 6, 9, and 12). Mean numbers of colonies ± SD are shown. The effects of *ARNT1* siRNAs were significant ($P < 0.02$). (*C*) Inhibitory effects of *ARNT1* siRNA on the expression of *CYP1A1* mRNA. Results of RT-PCR analysis with 10 nM control siRNA (lanes 4–6) or *ARNT* siRNA-1 (lanes 7–9) are shown. The RI of *ARNT1* mRNA is also given. (*D*) pSi^R-*ARNT1* restored protein expression. HuH-7 cells were introduced with control siRNA (lanes 1 and 2) or *ARNT1* siRNA-1 (lanes 3 and 4). On the next day, a control vector (C, lanes 1 and 3) or pSi^R-*ARNT1* (R, lanes 2 and 4) was transfected. Protein expression was detected by Western blot analysis on day 2 after the second transfection. (*E*) pSi^R-*ARNT1* recovered the L1-RTP suppressed by the siRNA. HuH-7 cells were transfected with *ARNT1* siRNA, followed by the introduction of a control vector (lanes 4–6) or pSi^R-*ARNT1* (lanes 7–9) on the following day. Then, cells were treated with 10 nM FICZ for 2 d followed by G418 selection. Mean numbers of colonies ± SD are shown. The difference between the number of Neo^R colonies obtained by pSi^R-*ARNT1* and by a control vector was significant ($P < 0.02$; compare lanes 6 and 9). C, control vector; D, 0.001% DMSO; F, 10 nM FICZ; R, pSi^R-*ARNT1*; U, untreated.

data indicated that FICZ mobilizes the L1 component to chromatin in a manner dependent on the activation of MAPK and ARNT1.

Discussion

In this study, we found that FICZ, a candidate physiological AhR ligand of a tryptophan photoproduct, induced L1-RTP. RNA-interference experiments conducted under strongly repressed expression of endogenous AhR suggested that AhR was not required for L1-RTP. In contrast, ARNT1, MAPK, and CREB were all involved in FICZ-induced L1-RTP. FICZ induced the association of ARNT1 and ORF1, and promoted the chromatin recruitment of ORF1 depending on the activation of MAPK. As the target of MAPK, CREB was pivotal for FICZ-induced L1-RTP, but our additional experiments revealed that the simple overexpression of a constitutively active form of *CREB* cDNA (p*CREB*^{Y134F}) (31) did not induce L1-RTP (Fig. S5). Additional functions of ARNT1 or MAPK are likely required for FICZ-induced L1-RTP.

We found that FICZ-induced L1-RTP was regulated in a fashion different from that induced by DNA double-strand breaks (DSB) (7). First, we observed that the time points of L1-RTP induced by FICZ and X-ray irradiation were different. In contrast, FICZ-induced L1-RTP was observed within 1–2 d (Fig. 1 *E* and *F*), but L1-RTP induced by DNA damage was observed only after 12 d of X-ray irradiation (Fig. S6*A*). Moreover, MAPK inhibitors

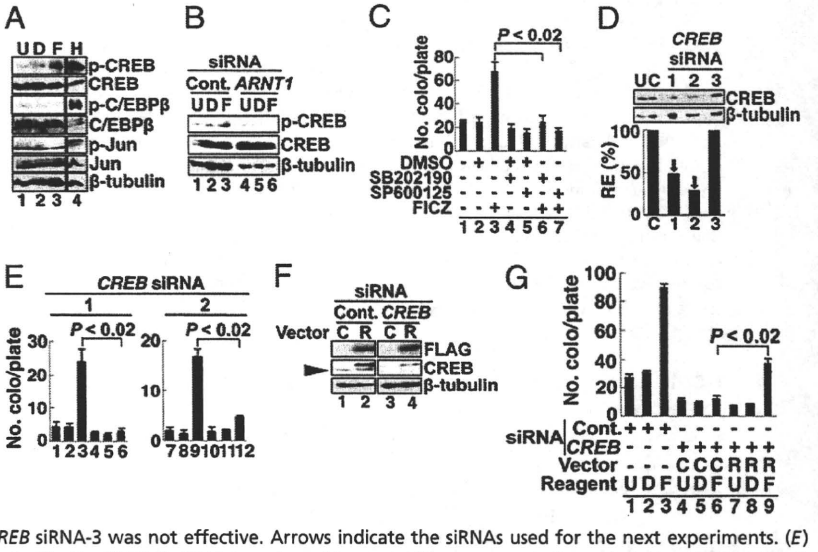

Fig. 4. MAPK and CREB are involved in L1-RTP. (*A*) Phosphorylation of CREB by FICZ. HuH-7 cells were treated with no reagents (U, lane 1), 0.001% DMSO (D, lane 2), 10 nM FICZ (F, lane 3), and 1 mM H_2O_2 (H, lane 4) as a positive control. Antibodies to nonphosphorylated or phosphorylated forms of CREB, C/EBP-β, and c-Jun were used. As a loading control, β-tubulin was detected. (*B*) FICZ-induced CREB phosphorylation depended on ARNT1. The FICZ-induced CREB phosphorylation was examined after introducing control siRNA (lanes 1–3) or *ARNT1* siRNA-1 (lanes 4–6). U, untreated (lanes 1 and 4); D, 0.001% DMSO (lanes 2 and 5); F, 10 nM FICZ (lanes 3 and 6). (*C*) Effects of MAPK inhibitors on L1-RTP. SB202190 (1 μM) and SP600125 (100 μM), which inhibit p38 and JNK, respectively, were added 30 min before the addition of 10 nM FICZ. Mean numbers of colonies ± SD are shown. The reductions in the numbers of Neo^R colonies by inhibitors were significant ($P < 0.02$; compare lanes 3, 6, and 7). (*D*) Functional evaluation of *CREB* siRNAs. First, dose responses of *CREB* siRNAs for the suppression of endogenous CREB were verified (Fig. S2*C*). Then, the activities of three different siRNAs (1–3) at 10 nM were examined. The RE of endogenous CREB protein was 48% and 28% when *CREB* siRNA-1 and -2 were introduced. *CREB* siRNA-3 was not effective. Arrows indicate the siRNAs used for the next experiments. (*E*) *CREB* siRNAs abrogated the L1-RTP. HuH-7 cells were transfected with 10 nM *CREB* siRNA-1 or -2, and treated with no reagents (lanes 1, 4, 7, and 10), 0.001% DMSO (lanes 2, 5, 8, and 11), or 10 nM FICZ (lanes 3, 6, 9, and 12). Then, a colony assay was carried out. Mean numbers of colonies ± SD are shown. *CREB* siRNA-1 (*Left*) and -2 (*Right*) significantly suppressed L1-RTP ($P < 0.02$). (*F*) pSi^R-*CREB* restored protein expression. HuH-7 cells were introduced with control siRNA (lanes 1 and 2) or *CREB* siRNA-1 (lanes 3 and 4) followed by transfection of a control vector (C) or pSi^R-*CREB* (R). CREB expression was checked on day 2 after transfection. Note that the band with a lower molecular weight is an endogenous CREB protein (lanes 1 and 2, arrowhead), which was abolished by *CREB* siRNA-1. (*G*) pSi^R-*CREB* recovered the L1-RTP suppressed by the siRNA. Experiments were performed as described (Fig. 3*E*). Mean numbers of colonies ± SD are shown. The difference between the number of Neo^R colonies recovered by pSi^R-*CREB* and a control vector was significant ($P < 0.02$; compare lanes 6 and 9). C, control vector; D, 0.001% DMSO; F, 10 nM FICZ; R, pSi^R-*CREB*; U, untreated.

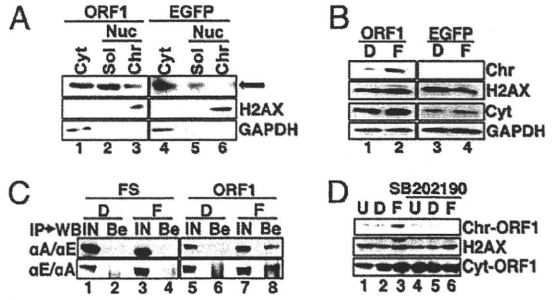

Fig. 5. The FICZ-induced chromatin recruitment of ORF1 depends on MAPK activity. (*A*) ORF1 present in the chromatin fraction. HuH-7 cells were transfected with plasmid DNAs encoding ORF1-TAP (lanes 1–3) or EGFP-TAP (lanes 4–6). On day 2 after transfection, cytoplasmic (Cyt, lanes 1 and 3), nuclear soluble (Sol, lanes 2 and 5), and chromatin (Chr, lanes 3 and 6) fractions were prepared and analyzed (*SI Methods*). H2AX and GAPDH were also detected to specify the subcellular localizations of the proteins. The arrow indicates the position of ORF1 in the chromatin fraction detected in lane 3. (*B*) Chromatin recruitment of ORF1 by FICZ. Similar experiments were done as described in *A*, and a chromatin fraction was prepared and analyzed 24 h after the addition of FICZ; 0.001% DMSO (D, lanes and 3); 10 nM FICZ (F, lanes 2 and 4). (*C*) FICZ stimulated the interaction of ARNT1 and ORF1. HuH-7 cells were transfected with p*FS-EGFP* (FS) (lanes 1–4) or p*ORF1-EGFP* (ORF1) (lanes 5–8). At 24 h after the addition of 0.001% DMSO (D, lanes 1, 2, 5, and 6) or 10 nM FICZ (F, lanes 3, 4, 7, and 8), cellular extracts were prepared and subjected to reciprocal experiments of immunoprecipitation (IP) followed by Western blot analysis (WB) (IP/WB). Upper row, IP with αARNT1 (αA) followed by WB using αE (αA/αE); lower row, IP with αEGFP (αE) followed by WB using αA (αE/αA). Both input sample (IN) (lanes 1, 3, 5, and 7) and protein recovered by protein G beads (Be) (lanes 2, 4, 6, and 8) were analyzed. As an IN sample, about one-tenth of the cell extract used for the IP was loaded. (*D*) MAPK inhibitor attenuated the chromatin recruitment of ORF1. SB202190 (1 μM) (lanes 4–6) was added 30 min before the addition of FICZ. U, untreated (lanes 1 and 4); D, 0.001% DMSO (lanes 2 and 5); F, 10 nM FICZ (lanes 3 and 6). ORF1 present in the chromatin fraction (Chr-ORF1 in top row) and cytoplasmic fraction (Cyt-ORF1 in bottom row) is shown. H2AX was also detected to specify the chromatin fraction (middle row). A similar result was obtained by an independent experiment.

completely blocked FICZ-induced L1-RTP (Fig. 4*C*), but not DSB-induced L1-RTP (Fig. S6*B*, lanes 7–9). Additionally, we found that TCDD was genotoxic, as judged by the increase of γ-H2AX (H2AX phosphorylated at serine 139), which is a sensitive cellular marker of DSB (32) (Fig. S6*C*, lanes 4 and 5), but it did not induce L1-RTP in HuH-7 cells (Fig. S6*D*), even though the same dose of TCDD induced the expression of CYP1A1 mRNA (Fig. S6*E*).

We carefully evaluated whether ARNT1 is a primary target involved in the rate-limiting process of FICZ-induced L1-RTP. Because XRE is present in the region of the 5′ UTR of human L1 (33) and mouse retroposons (34), we first excluded the possibility that FICZ induces L1-RTP by up-regulating the expression level of L1 mRNA. Quantitative RT-PCR analysis revealed that FICZ did not increase the expression of CMV-driven L1 mRNA (Fig. S7 *A* and *B*). Furthermore, MAPK inhibitors or siRNAs of *ARNT1* and *CREB* did not change the level of CMV-driven L1 mRNA (Fig. S7*B*, lanes 5–9). Additionally, FICZ did not increase the splicing efficiency of the immature L1 transcript (Fig. S7 *C* and *D*), *ORF2* mRNA (Fig. S7*E*), or the expression levels of ORF1/ORF2 proteins (Fig. S4 *B* and *D*). These findings strongly suggest that ARNT1 functions as the mediator for FICZ-induced L1-RTP.

ARNT1, as a central molecule of the class II bHLH/PAS proteins, either homodimerizes or promiscuously heterodimerizes with various bHLH/PAS members (9). As the best-characterized function, the NLS of ARNT1 contributes to nuclear trafficking of the ligand-bound AhR (11). Because ARNT1 has not been reported to function as a receptor to ligands, ARNT1 would likely associate with a novel molecule that binds FICZ. Interestingly, FICZ increases the mRNA expression of *Cry1* and *Cry2* genes, members of the bHLH/PAS family that are involved in the regulation of circadian rhythm (35). Furthermore, FICZ has been shown to change the electric activities of cells in the suprachiasmatic nucleus, where the master clock of circadian rhythm is maintained and controlled in response to light stimuli (36). These observations make it tempting to speculate that certain gene products involved in circadian rhythm can recognize FICZ, function as its receptor, and cooperate with ARNT1 for the induction of L1-RTP.

Our PCR-based assay revealed that picomolar levels of FICZ (3 pM) can induce L1-RTP (Fig. S8). About 8 pM FICZ was reported to be generated after a 24-h exposure of tissue-culture medium to ordinary laboratory light (14). Given that the concentration of tryptophan in human blood (about 70 μM) (37) is comparable to that present in tissue-culture medium (about 80 μM), FICZ may be generated in vivo and triggers L1-RTP. L1 is conserved in organisms from zebrafish to human (4), and a human L1 homolog of *Candida albicans* is competent for retrotransposition in *Saccharomyces cerevisiae* (38). Furthermore, cellular responses to FICZ have been reported in both a *Xenopus laevis* cell line (39) and zebrafish embryos (40), implying that FICZ can induce L1-RTP in various living organisms. Although further study is required, our current observations suggest the possibility that a member(s) of the bHLH/PAS family is involved in the epigenetic mode of L1-RTP. One possibility is that the genome shuffling by ARNT1-mediated L1-RTP provides living organisms the opportunity to acquire novel characteristics in response to environmental changes such as daylight.

Methods

Cells. HuH-7 cells (a human hepatocellular carcinoma cell line) and HeLa cells (a cervical carcinoma cell line) were used. The transfection efficiency of these cell lines, when judged by EGFP-positive cells after transfection of an *EGFP* expression vector, was about 70% and 30%, respectively.

L1-RTP Assays. Two different systems were used: a colony assay using pL1-Neo^R and a PCR-based assay using pEF06R. Each assay was performed at least twice, and representative results are presented. FICZ was used at 10 nM, unless stated otherwise.

RNA-Interference and Back-Transfection Experiments Using siRNA-Resistant Clones. Knockdown experiments were conducted using two different siRNAs for each gene. Each siRNA was used at 10 nM. To generate stringent conditions for down-regulated AhR expression, 50 nM *AhR* siRNA was used. Nucleotide sequences of used siRNAs were summarized in Table S1. The expression vectors for siRNA-resistant *ARNT1* and *CREB* cDNAs (pSi^R-*ARNT1* and pSi^R-*CREB*) and constitutively active CREB (p*CREB*^{Y134F}) were constructed based on pcDNA3.1 Zeo (+) (Invitrogen). Their quality was verified by restriction mapping and nucleotide sequencing.

Chromatin Recruitment of ORF1. Plasmid DNAs encoding *ORF1-TAP* (p*ORF1-TAP*) and *EGFP-TAP* (p*EGFP-TAP*) were generated using pcDNA3.1 Zeo. To prepare the DNA fragments, pBudORF1$_{syn}$ expressing a codon-optimized *ORF1* cDNA (29), pZome-1-C vector for *TAP-tag* cDNA (30), and pBOSH2BGFP-N1 for *EGFP* cDNA (41) were used.

Association of ORF1 and ARNT1. Plasmid DNAs encoding ORF1-EGFP (p*ORF1-EGFP*) and Flag-streptag EGFP (p*FS-EGFP*) were produced based on pcDNA3.1 Zeo. cDNA fragments were prepared from pBudORF1$_{syn}$ and pBOSH2BGFP-N1. p*FS-EGFP* was prepared by inserting an oligonucleotide cassette encoding -WSHPQFEK-WSHPQFEK-M- (amino acid sequence for 2xstreptag peptide is depicted by single letters, with spacers indicated by "-") into 5′ to *EGFP* cDNA that had been inserted in pFlag-CMV2 (Sigma).

Statistics. Statistical significance was evaluated using the Mann–Whitney *U* test. A *P* value of <0.05 was considered to be statistically significant.

Experimental procedures and construction of the plasmid DNAs are described in detail in *SI Methods*.

ACKNOWLEDGMENTS. We are grateful to Drs. Nicolas Gilbert (University of Michigan Medical School, Ann Arbor, MI), Eline T. Luning Prak (University of Pennsylvania School of Medicine, Philadelphia, PA), John Goodier (University of Pennsylvania School of Medicine, Philadelphia, PA), Gabriele Vielhaber (Symrise, Holzminden, Germany), Mark Hahn (Woods Hole Oceanographic Institution, Woods Hole, MA), Oliver Hankinson (Jonsson Comprehensive Cancer Center, University of California, Los Angeles, CA), Kumiko Saeki (National Center for Global Health and Medicine), Astrid M. Roy-Engel (Tulane University Health Sciences Center, New Orleans, LA), and Geoffrey M. Wahl (Salk Institute for Biological Studies, La Jolla, CA) for providing us with pCEP4/L1*mneol*/ColE1, pEF06R, an antibody to ORF2, MNF, an antibody to AhRR, *ARNT1* cDNA, *CREB* cDNA, pBudORF1$_{syn}$/ORF2$_{syn}$, and pBOSH2BGFP-N1. Dr. Takuro Shimbo (National Center for Global Health and Medicine) kindly carried out statistical analysis of experimental data. This work was supported by a grant from the National Center for Global Health and Medicine (21A-104) and in part by a research grant for the Long-Range Research Initiative from the Japan Chemical Industry Association.

1. Bannert N, Kurth R (2004) Retroelements and the human genome: New perspectives on an old relation. *Proc Natl Acad Sci USA* 101 (Suppl 2):14572–14579.
2. Kazazian HH, Jr (2004) Mobile elements: Drivers of genome evolution. *Science* 303: 1626–1632.
3. Goodier JL, Kazazian HH, Jr (2008) Retrotransposons revisited: The restraint and rehabilitation of parasites. *Cell* 135:23–35.
4. Furano AV, Duvernell DD, Boissinot S (2004) L1 (LINE-1) retrotransposon diversity differs dramatically between mammals and fish. *Trends Genet* 20:9–14.
5. Brouha B, et al. (2003) Hot L1s account for the bulk of retrotransposition in the human population. *Proc Natl Acad Sci USA* 100:5280–5285.
6. Han JS, Szak ST, Boeke JD (2004) Transcriptional disruption by the L1 retrotransposon and implications for mammalian transcriptomes. *Nature* 429:268–274.
7. Farkash EA, Kao GD, Horman SR, Luning Prak ET (2006) Gamma radiation increases endonuclease-dependent L1 retrotransposition in a cultured cell assay. *Nucleic Acids Res* 34:1196–1204.
8. Hahn ME (2002) Aryl hydrocarbon receptors: Diversity and evolution. *Chem Biol Interact* 141:131–160.
9. Kewley RJ, Whitelaw ML, Chapman-Smith A (2004) The mammalian basic helix-loop-helix/PAS family of transcriptional regulators. *Int J Biochem Cell Biol* 36:189–204.
10. Denison MS, Nagy SR (2003) Activation of the aryl hydrocarbon receptor by structurally diverse exogenous and endogenous chemicals. *Annu Rev Pharmacol Toxicol* 43:309–334.
11. Eguchi H, Ikuta T, Tachibana T, Yoneda Y, Kawajiri K (1997) A nuclear localization signal of human aryl hydrocarbon receptor nuclear translocator/hypoxia-inducible factor 1β is a novel bipartite type recognized by the two components of nuclear pore-targeting complex. *J Biol Chem* 272:17640–17647.
12. Beischlag TV, Luis Morales J, Hollingshead BD, Perdew GH (2008) The aryl hydrocarbon receptor complex and the control of gene expression. *Crit Rev Eukaryot Gene Expr* 18:207–250.
13. Rannug A, et al. (1987) Certain photooxidized derivatives of tryptophan bind with very high affinity to the Ah receptor and are likely to be endogenous signal substances. *J Biol Chem* 262:15422–15427.
14. Oberg M, Bergander L, Håkansson H, Rannug U, Rannug A (2005) Identification of the tryptophan photoproduct 6-formylindolo[3,2-*b*]carbazole, in cell culture medium, as a factor that controls the background aryl hydrocarbon receptor activity. *Toxicol Sci* 85:935–943.
15. Wincent E, et al. (2009) The suggested physiologic aryl hydrocarbon receptor activator and cytochrome P4501 substrate 6-formylindolo[3,2-*b*]carbazole is present in humans. *J Biol Chem* 284:2690–2696.
16. Fritsche E, et al. (2007) Lightening up the UV response by identification of the arylhydrocarbon receptor as a cytoplasmatic target for ultraviolet B radiation. *Proc Natl Acad Sci USA* 104:8851–8856.
17. Quintana FJ, et al. (2008) Control of T(reg) and T(H)17 cell differentiation by the aryl hydrocarbon receptor. *Nature* 453:65–71.
18. Veldhoen M, et al. (2008) The aryl hydrocarbon receptor links TH17-cell-mediated autoimmunity to environmental toxins. *Nature* 453:106–109.
19. Saeki K, Saeki K, Yuo A (2003) Distinct involvement of cAMP-response element-dependent transcriptions in functional and morphological maturation during retinoid-mediated human myeloid differentiation. *J Leukoc Biol* 73:673–681.
20. Moran JV, et al. (1996) High frequency retrotransposition in cultured mammalian cells. *Cell* 87:917–927.
21. Hoffman EC, et al. (1991) Cloning of a factor required for activity of the Ah (dioxin) receptor. *Science* 252:954–958.
22. Baba T, et al. (2001) Structure and expression of the Ah receptor repressor gene. *J Biol Chem* 276:33101–33110.
23. Dougherty EJ, Pollenz RS (2008) Analysis of Ah receptor-ARNT and Ah receptor-ARNT2 complexes in vitro and in cell culture. *Toxicol Sci* 103:191–206.
24. Kwon M-J, Jeong K-S, Choi EJ, Lee BH (2003) 2,3,7,8-Tetrachlorodibenzo-*p*-dioxin (TCDD)-induced activation of mitogen-activated protein kinase signaling pathway in Jurkat T cells. *Pharmacol Toxicol* 93:186–190.
25. Lee HE, et al. (2009) Biphasic activation of p38MAPK suggests that apoptosis is a downstream event in pemphigus acantholysis. *J Biol Chem* 284:12524–12532.
26. Bennett BL, et al. (2001) SP600125, an anthrapyrazolone inhibitor of Jun N-terminal kinase. *Proc Natl Acad Sci USA* 98:13681–13686.
27. Bain J, McLauchlan H, Elliott M, Cohen P (2003) The specificities of protein kinase inhibitors: An update. *Biochem J* 371:199–204.
28. Goodier JL, Zhang L, Vetter MR, Kazazian HH, Jr (2007) LINE-1 ORF1 protein localizes in stress granules with other RNA-binding proteins, including components of RNA interference RNA-induced silencing complex. *Mol Cell Biol* 27:6469–6483.
29. Wallace N, Wagstaff BJ, Deininger PL, Roy-Engel AM (2008) LINE-1 ORF1 protein enhances Alu SINE retrotransposition. *Gene* 419:1–6.
30. Rigaut G, et al. (1999) A generic protein purification method for protein complex characterization and proteome exploration. *Nat Biotechnol* 17:1030–1032.
31. Du K, Asahara H, Jhala US, Wagner BL, Montminy M (2000) Characterization of a CREB gain-of-function mutant with constitutive transcriptional activity in vivo. *Mol Cell Biol* 20:4320–4327.
32. Rogakou EP, Pilch DR, Orr AH, Ivanova VS, Bonner WM (1998) DNA double-stranded breaks induce histone H2AX phosphorylation on serine 139. *J Biol Chem* 273: 5858–5868.
33. Stribinskis V, Ramos KS (2006) Activation of human long interspersed nuclear element 1 retrotransposition by benzo(a)pyrene, an ubiquitous environmental carcinogen. *Cancer Res* 66:2616–2620.
34. Roman AC, Benitez DA, Carvajal-Gonzalez JM, Fernandez-Salguero PM (2008) Genome-wide B1 retrotransposon binds the transcription factors dioxin receptor and Slug and regulates gene expression in vivo. *Proc Natl Acad Sci USA* 105:1632–1637.
35. Mukai M, Tischkau SA (2007) Effects of tryptophan photoproducts in the circadian timing system: Searching for a physiological role for aryl hydrocarbon receptor. *Toxicol Sci* 95:172–181.
36. Reppert SM, Weaver DR (2002) Coordination of circadian timing in mammals. *Nature* 418:935–941.
37. Suzuki Y, et al. (2010) Increased serum kynurenine/tryptophan ratio correlates with disease progression in lung cancer. *Lung Cancer* 67:361–365.
38. Dong C, Poulter RT, Han JS (2009) LINE-like retrotransposition in *Saccharomyces cerevisiae*. *Genetics* 181:301–311.
39. Laub LB, Jones BD, Powell WH (2010) Responsiveness of a *Xenopus laevis* cell line to the aryl hydrocarbon receptor ligands 6-formylindolo[3,2-*b*]carbazole (FICZ) and 2,3,7,8-tetrachlorodibenzo-*p*-dioxin (TCDD). *Chem Biol Interact* 183:202–211.
40. Jönsson ME, et al. (2009) The tryptophan photoproduct 6-formylindolo[3,2-*b*] carbazole (FICZ) binds multiple AHRs and induces multiple *CYP1* genes via AHR2 in zebrafish. *Chem Biol Interact* 181:447–454.
41. Kanda T, Sullivan KF, Wahl GM (1998) Histone-GFP fusion protein enables sensitive analysis of chromosome dynamics in living mammalian cells. *Curr Biol* 8:377–385.